Konrad-Zuse-Zentrum für Informationstechnik Berlin
Heilbronner Str. 10, D-10711 Berlin - Wilmersdorf

Jochen Fröhlich and Jens Lang

Twodimensional Cascadic Finite Element Computations of Combustion Problems

Preprint SC 96-5 (February 1996)

Twodimensional Cascadic Finite Element Computations of Combustion Problems

JOCHEN FRÖHLICH AND JENS LANG

ABSTRACT

We present an integrated time–space adaptive finite element method for solving systems of twodimensional nonlinear parabolic systems in complex geometry. The partial differential system is first discretized in time using a singly linearly implicit Runge–Kutta method of order three. Local time errors for the step size control are defined by an embedding strategy. These errors are used to propose a new time step by a PI controller algorithm. A multilevel finite element method with piecewise linear functions on unstructured triangular meshes is subsequently applied for the discretization in space. The local error estimate of the finite element solution steering the adaptive mesh refinement is obtained solving local problems with quadratic trial functions located essentially at the edges of the triangulation. This two–fold adaptivity successfully ensures an a priori prescribed tolerance of the solution. The devised method is applied to laminar gaseous combustion and to solid–solid alloying reactions. We demonstrate that for such demanding applications the employed error estimation and adaption strategies generate an efficient and versatile algorithm.

KEY WORDS: Adaptive Finite Elements, Embedded Runge–Kutta Methods, A Posteriori Error Estimates, Reaction–Diffusion Equations, Solid–Solid Reaction.

AMSMOS, MSC 1991 SUBJECT CLASSIFICATION:
Primary 65M60; Secondary 35K57, 80A32, 65M50.

*Konrad–Zuse–Zentrum Berlin, Heilbronner Str. 10, D–10711 Berlin, Germany.

1 Introduction

Even with the dramatical increase of available computing power observed today a lot of physically relevant problems still remain inaccessible to a numerical solution. This is mostly due to the large complexity that realistic mathematical models involve. In most cases the information is highly nonuniformly distributed in space and time. This can be due to different reasons such as complex geometry, sudden changes in boundary conditions or coefficients and in particular stiff operators. In such a situation it is crucial to dispose of an adaptive discretization method. Not only it brings the solution within reach by drastically reducing the number of degrees of freedom, but also furnishes error bounds and thus permits to estimate its reliability which may be as important as the solution itself. The present paper is concerned with an adaptive method in both, space and time.

Combustion problems are known to range among the most demanding for spatial adaptivity when the thin flame front is to be resolved numerically. This is often required as the inner structure of the flame determines global properties such as the flame speed, the formation of cellular patterns or even more important the mass fraction of reaction products (e.g. NO_x formation). A large part of numerical studies in this field is devoted to the different instabilities of such flames exhibiting cellular, pulsating, spiraling, etc. to name but a few, and often transition to chaotic behaviour [PW82], [DLP89], [FP91], [DH92]. Apart from spatial adaptivity these problems can generally be solved with a constant time step. A reliable error control as available with the present method, however, is of great advantage. When dealing with ignition and extinction processes or complicated geometries and non–uniform material the relevant time scales can change by orders of magnitude. The proposed method then automatically adjusts the time step in accordance with the spatial tolerance so that the invested computational effort results in an optimal advancement of the calculation in time. A crucial point is that, apart from the choice of the overall precision, the algorithm does not require the adjustment of tuning parameters when changing from one problem to another. This is a major advantage with respect to many other methods and thereby simplifies its applicability to new problems.

The literature on adaptive space discretization and adaptive time discretization is abundant. For a survey on these topics the reader is refered to [HW91], [BS90], [Ver94], [DLN96]. A successfull approach to many problems requiring adaptive discretization in space is constituted by the Multilevel Finite Element (MLFE) method proposed in [DLY89]. Time dependent parabolic problems are then adequately handled by the TS–discretization sequence (first time then space) as it reduces the problem to the solution of elliptic sub–problems. In opposite to the widely used Method Of Lines (MOL) approach [BB82], [AF88], [Moo94] the adaptation in space is thus placed in the interiour of the time steps. This so–called Rothe method was first developed and analyzed in [Bor92] for linear problems and later extended to the nonlinear case in [LW92] using linearly implicit Runge–Kutta schemes. The resulting algorithm has demonstrated its reliability for a variety of unsteady reaction–diffusion problems [Lan95], [Lan96]. In particular for problems where the main complexity is generated by spatial nonuniformity the applied discretization sequence can be advantageous. We finally note that a new adaptive multilevel discretization in space by means of orthogonal wavelets has been obtained recently and applied to the equations solved in Section 3 [FS95].

In the present paper we focuss on the adaptive MLFE computation of twodimensional combustion processes. These include many challenging practically relevant problems that request several improvements with respect to our earlier work mentioned above. Dealing with large problems these may become crucial for the efficient application of the developed methodology. The equations which are solved are of reaction–diffusion type. It should be noted that a large number of phenomena in biology, ecology, physics and engineering are governed by equations of this type. The current implementation permits to handle systems of an arbitrary number of such equations. It furthermore allows to impose additional algebraic or differential-algebraic constraints, a feature not required in the present study. Finally, the extension to account for mild convection does not pose problems and is available as well. Hence, the developed algorithm indeed has a wide range of applications.

The paper is laied out as follows. In section 2 we present the MLFE algorithm and the adaption strategy in time. In particular, an improved prediction formula yields a smooth and satisfactory behaviour of the time step. We then present results for laminar thermodiffusive flames impinging on an obstacle. The second class of applications is constituted by solid–solid alloying reactions. We define an illustrative setup for which detailed results are presented.

2 Time and Space Discretization

The equations considered here are special cases of the following class of semilinear diffusion problems:

$$\begin{aligned} P(x)\partial_t u \;+\; A(\partial_x, x)\, u &= F(u)\,, \qquad x \in \Omega,\ t > 0 \\ u(0,x) &= u_0(x)\,, \qquad x \in \Omega\,, \end{aligned} \tag{2.1}$$

where u is the $d-$dimensional vector of dependent variables. P is an x–dependent $d \times d$–matrix and A is a linear elliptic differential operator of second order with respect to the spatial variable x. In the present applications the functions u, u_0 and F are vectors of two real functions. The computational domain $\Omega \subset \mathbb{R}^2$ is bounded, and appropriate boundary conditions on $\partial\Omega$ are assumed to be incorporated into the operator A. In [Lan95] a time–space adaptive method for (2.1) has been described in a general setting. In the sequel we recall some essential features and focus on new aspects for our case.

Combustion problems are generally characterized by the presence of different time scales. They originate from ignition processes, travelling flame fronts or fast and slow reactions of the chemical species. This makes the whole system temporally very stiff so that such problems are best treated with an implicit or semi–implicit time discretization. Due to rich spatial dynamics frequent adaptation of the spatial grid is necessary as well. Consequently, time integrators using a wide stencil of different time levels to construct higher order solutions such as multistep or extrapolation methods seem not to be favorable here as the spatial discretization is permanently changing. In such a situation one–step Runge–Kutta methods requiring only two different meshes, one to construct the new solution and one to hold the initial values on the old time level, have a structural advantage. Additionally, they are able to avoid nonlinear systems employing a fixed sequence of linear problems. These algorithms are often called linearly implicit Runge–Kutta methods. We employ a singly diagonally implicit method which has shown to give very satisfactory results for stiff equations. Setting

$$f(u) := F(u) - A(\partial_x, x)u \tag{2.2}$$

the semi–discretization of (2.1) in time is based on the stage values $l_j, j = 1,2,3$ determined by

$$\left(\frac{1}{\gamma\ \tau_n} P - \partial_u f(u_{n-1})\right) l_j = f(\, u_{n-1} + \sum_{i=1}^{j-1} a_{ji}\, l_i\,) + \frac{1}{\tau_n}\, P \sum_{i=1}^{j-1} c_{ji}\, l_i \tag{2.3}$$

The time scheme then relates the approximate solution u_n at time t_n to the known value u_{n-1} with a time step $\tau_n = t_n - t_{n-1}$ through

$$u_n = u_{n-1} + \sum_{j=1}^{3} b_j\, l_j\ . \tag{2.4}$$

Observe that the sums in the right–hand side extend to $j-1$ only which results in a successive solution process. The coefficients γ, a_{ji}, c_{ji} and b_j are choosen such that u_n is of third order in time, and furthermore to give good stability properties [Roc88]. As outlined above the adaptive choice of the time step is an important feature for an efficient solution process. It is thus necessary to incorporate an estimate of the local error in time. The special structure of the employed Runge–Kutta scheme allows the definition of a lower order solution by an embedding strategy. We simply employ a different set of coefficients in (2.4) to yield a solution of second order

$$\hat{u}_n = u_{n-1} + \sum_{j=1}^{3} \hat{b}_j\, l_j\ . \tag{2.5}$$

The difference between the solutions of different order is then used to estimate the local error in time

$$\epsilon_n \ := \ \|u_n - \hat{u}_n\|_\Omega\ . \tag{2.6}$$

In practical applications it is often decisive to carefully choose the norm. It should accurately reflect the scale of the problem in order to furnish meaningful input for the error control. We employ here the weighted L_2–norm

$$\|u_n - \hat{u}_n\|_\Omega \ := \ \left(\frac{1}{d}\sum_{i=1}^{d} \frac{\|\hat{u}_{n,i} - u_{n,i}\|_0^2}{w_i^2}\right)^{1/2} \tag{2.7}$$

where $u_{n,i}$ denotes the $i-$th component of u_n. Extensive practical experience leads us to employ the reference quantities

$$w_i := \begin{cases} ABS_i & : \quad \|u_{n,i}\|_0 < ABS_i \\ REL_i & : \quad ABS_i \leq \|u_{n,i}\|_0 < REL_i \\ \|u_{n,i}\|_0 & : \quad REL_i \leq \|u_{n,i}\|_0 \end{cases} \tag{2.8}$$

with

$$\begin{aligned} REL_i &:= RTOL_i * \max_n \|u_{n,i}\|_0 \; , \\ ABS_i &:= ATOL_i * |\Omega|^{1/2} \; . \end{aligned} \tag{2.9}$$

and $|\Omega|$ the size of the considered domain. Given a tolerance TOL_t for the time discretization a standard strategy is to choose the step size of the time step according to

$$\tau_n \;:=\; \rho \left(\frac{TOL_t}{\epsilon_{n-1}} \right)^{1/3} \tau_{n-1} \; , \tag{2.10}$$

where ρ denotes a safety factor, presently set to be 0.95. The exponent in (2.10) results from the cubic model for the local error in time which is supposed to underly. The step is then executed and the error ϵ_n from (2.6) is checked to be smaller than TOL_t. If this is not the case the solution u_n is rejected and the time step is repeated with a reduced value of τ_n. Unfortunately, this mechanism often leads to a nonsmooth behavior of the time integration process. For instance, after a drastic step size reduction the corresponding error ϵ becomes very small. Consequently, the proposed new time step will be too optimistic leading to repeated rejections. One possible remedy is to smooth out the step size selection using a PI controller as introduced in [Gus92] for implicit methods. It takes the form

$$\tau_n := \rho \, \frac{\tau_{n-1}}{\tau_{n-2}} \left(\frac{TOL_t}{\epsilon_{n-1}} \frac{\epsilon_{n-2}}{\epsilon_{n-1}} \right)^{1/3} \tau_{n-1} \; . \tag{2.11}$$

and is used in case of more than two successively accepted time steps. If time steps are rejected relation (2.10) is used with several modifications. The error information resulting from the rejected steps can e.g. be used to modify the exponent in (2.10) which in that case apparently does not correspond to what really happens.

Let us now consider the spatial discretization. In (2.3) it is obvious that for the three stage values l_j three linear elliptic boundary value problems have to be solved. This is being done by a multilevel finite element method (MFEM). In the spirit of full adaptivity, a self–adaptive spatial discretization method is an appropriate choice for this task. It has proven to be a useful tool for drastically reducing the size of the arrising linear systems and to achieve high and controlled accuracy. The general principle of the multilevel technique consists of replacing the solution space by a sequence of discrete spaces with successively increasing dimensions to improve the approximation property [DLY89]. At the same time this speeds up the iterative solution of linear systems through the possible use of nested iterations. An MFEM requires the specification of four modules: the finite element assembly, the estimation technique for the error in space, the mesh refinement strategy, and last but not least the solver for the linear equations. These steps are now described in detail.

The starting point for any FEM is the weak formulation of the corresponding boundary value problem. The stage problems (2.3) are equivalent to the variational formulation

$$B_\tau(l_j, v) \;=\; r_j(v) \qquad \text{for all } v \in V,\ j = 1, 2, 3, \tag{2.12}$$

where B_τ denotes the time–dependent bilinear form associated with the operator on the left–hand side of (2.3), r_j stands for the corresponding right–hand side operator of the j–th stage, and V is a subspace of the Sobolev space $[H^1(\Omega)]^d$, containing the solution $u \in I\!R^d$. We presently use a conforming FE–discretization without slave nodes based on piecewise linear polynomials and triangular grids. Let T_0 be the initial triangulation of the domain Ω. Then a sequence of nested triangulations $T_0, T_1, \ldots, T_j$ is constructed by successive local refinement. Clearly, new grid points should be placed only in those regions where the current precision is insufficient. For this procedure it is required that the spatial discretization error can be estimated for each triangle of T_k. It is then used to select a set R_k of triangles which have to be refined. Refining all triangles of R_k into four congruent triangles ("red" refinement) has proven to be a robust strategy in many applications. To ensure that the new triangulation T_{k+1} does not possess slave nodes, triangles with one refined edge are subdivided into two triangles ("green" refinement), those with two or three refined edges are refined "red". Recall that the finite element discretization error grows when the maximal angle tends to π [BA76]. Moreover, since the condition number of the stiffness matrix increases like $1/\sin(\alpha)$, where α is the minimal angle, it is important to bound the angles away from 0 and π. Pure "red" refinement guarantees this immediately as the triangles in each T_k are congruent to those in T_0. In order to avoid degeneration due to repeated "green" refinement the "green" closures of each triangulation are removed before refining. This refinement strategy is standard and used e.g. in the KASKADE code [ELR93].

Each triangulation T_k corresponds to a finite element subspace V_k of V consisting of all continuous functions which are linear on each triangle $T \in T_k$. The finite element solutions $l_j^k \in V_k,\ j = 1, 2, 3$, on T_k have now to satisfy the equation (2.12) restricted to the related subspace V_k

$$B_\tau(l_j^k, v) \;=\; r_j(v) \qquad \forall\, v \in V_k,\ j = 1, 2, 3\,,\ k = 1, 2, \ldots. \tag{2.13}$$

Once the approximate solutions have been computed, a posteriori error estimators can be utilized to give specific assessment of the error distribution. With the above time integrator, the new solution u_n^k on the triangulation T_k is obtained by solving three different stage problems for l_j^k in V_k, (2.13). An estimation process for the discretization error in space which includes all these problems would become too expensive. A natural way therefore is to use the first stage only, justified by the fact that

$$u_{Euler}^k \;:=\; u_{n-1} + l_1^k/\gamma \tag{2.14}$$

is exactly the semi–implicit Euler solution of (2.1) at $t = t_n$ on the triangulation T_k. Hence, it can be assumed that a spatial mesh well–fitted to u^k_{Euler} is appropriate for l_1, l_2, l_3 and u_n in (2.3), (2.4). Observe that there are two contributions to the spatial error of u^k_{Euler}. One results from l^k_1, the other from the fact that fine grid components of u_{n-1} can not be represented on those parts of the grid T_k where the latter is coarser than the grid of the previous time step. They are respectively termed δ_l and δ_u in the sequel.

The current error estimation techniques can roughly be devided into two categories. The first ones are interpolation methods which play an important role in the traditional finite element approximation theory. In [Lan95] such a technique has been studied for the above problem class. The computed quantities can be very useful and relatively cheap error indicators for adaptive grid improvement in many cases. Unfortunately, the involved error constants to be specified a priori for a general class of solutions may or may not yield too pessimistic estimations for the actual error. Although this can be compensated for simple problems by appropriate adjustments it is a severe drawback under more complex conditions characterized, e.g., by non–constant properties and highly unsteady solutions as encountered in the examples below.

We therefore employ a second type of error estimator based on the computation of approximate local residuals. This requires higher order approximations of local solutions and thus strongly depends upon the governing operators. In general these estimators are much more expensive than the first ones. On the other hand they produce quite accurate and robust estimates of the discretization error. For further information we refer e.g. to the survey of Noor and Babuška [NB87]. With such an approach an estimate of the local spatial discretization error of a stage value l^k (on the grid T_k) is obtained by solving a set of local problems on small subdomains $\omega_i \subset \Omega$. For clarity we first consider a single subproblem and drop the index i. In the spirit of Babuška and Rheinboldt [BR78] the local error $\delta_l = l_1 - l^k_1 \in [H^1_0(\omega)]^d$ is determined imposing homogenous Dirichlet boundary conditions so that δ_l is solution of

$$\begin{aligned} B_\tau(\delta_l, v) &= r_1(v) - B_\tau(l^k_1, v) \qquad && \forall v \in [H^1_0(\omega)]^d \,, \\ \delta_l(x) &= 0 \,,\ x \in \partial\omega \,, && \text{if } \partial\omega \cap \partial\Omega = \emptyset \,, \end{aligned} \tag{2.15}$$

If $\partial\omega \cap \partial\Omega$ is non–empty the boundary conditions have in general to be modified according to the boundary conditions on $\partial\Omega$. In the computations below an edge–based error estimator is employed choosing ω to be the union of the adjacent triangles to an edge E of T_k. The subproblem (2.15) is then discretized by restricting v to $Q(\omega)$, the space of quadratic polynomials on ω. The local spatial error can thus be represented by only one degree of freedom for each component of the solution vector situated at the midpoint of the corresponding edge E. Hence, the local solution is determined through a small $d \times d$ system only. Similarly, the local error of the old solution u_{n-1} restricted to T_k is approximated as

$$\delta_u = \Big(u_{n-1}(x_m) \; - \; u^k_{n-1}(x_m) \Big) \; v_E \tag{2.16}$$

where $v_E \in Q(\omega)$ is the quadratic finite element function with respect to the midpoint

x_m of the edge E. Finally, the local error of u^k_{Euler} in (2.14) is estimated as

$$\eta := \|\delta_u \;+\; \delta_l/\gamma\|_\omega \tag{2.17}$$

employing the norm defined in (2.7). This expression is an asymptotically upper bound for the norm of the true local error. Note that different error estimators of the above type can be devised either by increasing the size of the domain ω [Mit89] or by choosing a different discretization of the local error δ_l [BW85]. The extensive comparison in [Mit89] showes however that the increased effort for better estimation through a local problem with more degrees of freedom often does not pay off.

In the estimation step of the algorithm the above local procedure is applied all over the computational domain, in our case to all ω_i defined by the edges of T_k. In order to produce a nearly optimal finite element mesh, edges having an error η_i^2 larger than the mean square value are refined. This technique equilibrates the local error over the whole mesh in several iterations and improves the finite element solution locally until a fixed spatial tolerance

$$\left(\sum_i \eta_i^2\right)^{1/2} \le \; TOL_x \tag{2.18}$$

is achieved. The relationship between spatial and temporal accuracy in the fully nonlinear approach is studied in [LW92]. Given a prescribed global tolerance TOL we use

$$TOL_x = TOL/3.0 \quad \text{and} \quad TOL_t = TOL/2.0\;.$$

The linear system arising from each of the refined grids T_k is set up and solved by the BICGSTAB algorithm preconditioned with an SSOR method. Its convergence behaviour is very smooth and in most cases it converges considerably faster than other methods. This iterative procedure is speeded up at every refinement level k using the solution of the previous (coarser) level $k-1$ as initial value. To summarize this section, Fig. 1 gives a flow diagram of the whole adaptive iteration process.

3 Laminar flames through an obstacle

The major part of gaseous combustion processes can adequately be described under the low Mach number hypothesis. This essentially amounts to eliminating the pressure dependence of the fluid density while retaining its temperature dependence. When the latter is not accounted for neither, the motion of the fluid becomes independent from temperature and species concentration. What remains is that the velocity field influences these quatities via a convection term. Hence, one can solve the temperature and species equations alone specifying any solenoidal velocity field $u(x,t)$. In particular, $u = 0$, $u = u_0 = const.$, and $u = -u_f$ with $u_f(t)$ being the velocity of the flame front are important cases. Introducing the dimensionless temperature $\theta = (T - T_{unburnt})/(T_{burnt} - T_{unburnt})$,

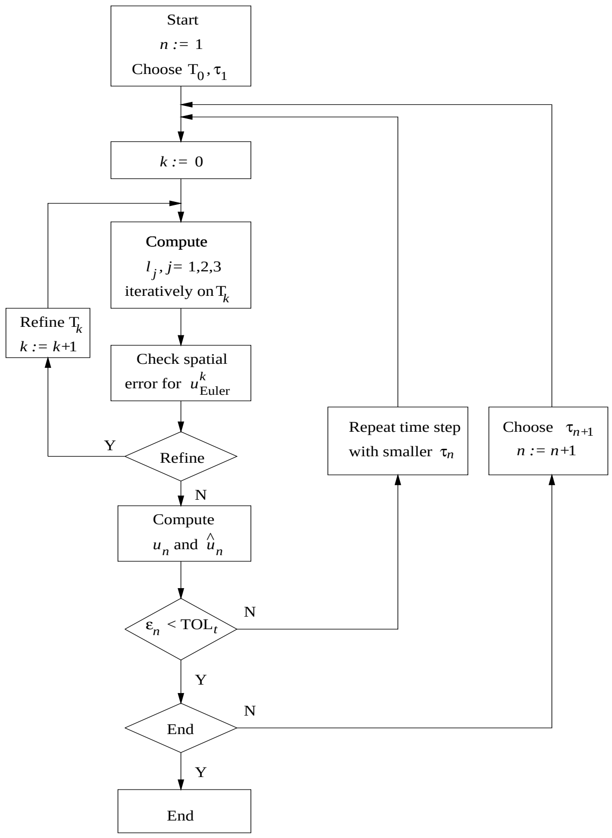

FIG. 1. Flow chart for the time-space adaptive solver KARDOS.

denoting by Y the species concentration, and assuming constant diffusion coefficients yields [Pet82]

$$\partial_t \theta - \quad \nabla^2 \theta \quad = \quad \omega \tag{3.1}$$

$$\partial_t Y - \frac{1}{Le} \nabla^2 Y \quad = \quad -\omega \tag{3.2}$$

where the Lewis number Le is the ratio of diffusivity of heat and diffusivity of mass. The time has been nondimensionalized with the heat conduction time scale, and the heat release parameter has entered in the reaction term through the definition of θ. We use a simple one-species reaction mechanism governed by an Arrhenius law

$$\omega \ = \ \frac{\beta^2}{2Le} \, Y \, e^{\frac{-\beta(1-\theta)}{1+\alpha(1-\theta)}} \tag{3.3}$$

in which an approximation for large activation energy has been employed [BF70]. The temperature ratio $\alpha = (T_{burnt} - T_{unburnt})/T_{burnt}$ is the quantity that determines the gas expansion in non-constant density flows so that the above thermo-diffusive modell is exact for $\alpha = 0$. The extension of (3.1), (3.2) to a complex reaction scheme is straightforward by adding similar equations for additional species and modifying the reaction terms. We have also performed computations with an additional convection term. This can either describe the response of a thermodiffusive flame to a given velocity field under fixed boundary conditions or it can be used to furnish a moving reference frame (equivalent to dynamic regridding) in which a propagating flame front may become stationary. In the latter case the spatially uniform velocity is chosen proportional to the instantaneous integral of the reaction rate.

In this section we consider a freely propagating laminar flame described by eqs. (3.1), (3.2) and its response to a heat absorbing obstacle, e.g. a cooled grid. It covers half the chanel width and is one diameter long. The absorbtion of heat is modelled by the boundary condition

$$\partial_n \theta \;=\; -\, k\,(\theta - \theta_{ref}) \tag{3.4}$$

where k is a heat loss parameter and where the reference temperature is chosen as $\theta_{ref} = \theta_{unburnt} = 0$. On the left boundary of the domain (cf. Fig. 2) Dirichlet conditions corresponding to the burnt state are prescribed while the remaining boundary conditions are of homogeneous Neuman type. The initial condition is the analytical solution of a onedimensional right-travelling flame in the limit $\beta \to \infty$ located left of the obstacle.

Two different situations may occur in this experiment according to the value of k. For small k the flame becomes curved and is slowed down in the interiour of the chanel but manages to pass through. For stronger heat loss the flame is extinguished. Computations of this phenomenon in a simple chanel geometry have been done in [BDL89]. In the present setting the extinction limit is a function of many parameters: length and width of the obstacle, its geometry, the Lewis number, the type of boundary condition and the amount of heat loss. We therefore do not aim here at determining precise thresholds but rather show a sample computation for each of the two regimes choosing $Le = 1$, $\beta = 10$, $\gamma = 0.8$. Appart from information on the physical mechanism these illustrate the performance and the robustness of the employed numerical method.

Fig. 2 reports a computation with heat loss below the critical value. Part a)–d) show the propagation of the reaction front. To our experience the reaction rate is by far the best quantity to judge on adequate spatial resolution of such a computation, as it is related to the smallest spatial scales of the problem. The present results show (backed by additional verifications) that ω is indeed well–resolved although being controlled only indirectly through the adaption process based on θ and Y. Fig. 3 displays grid and lines of constant temperature for $t = 20$ to give an impression of these as well. The former contains about 2000 nodes resulting from a tolerance $TOL = 10^{-2}$. Fig. 4 depicts reaction rate and time step during the propagation. When the flame passes through the chanel the total reaction rate diminishes not only due to the smaller width of the front but also due to heat loss. The peak near the endof the graph results from increased flame area after the front leaves the obstacle. According to the temporally reduced flame velocity the time step automatically increases about one order of magnitude. This results in essential savings of computation time with respect to a constant time step. The latter

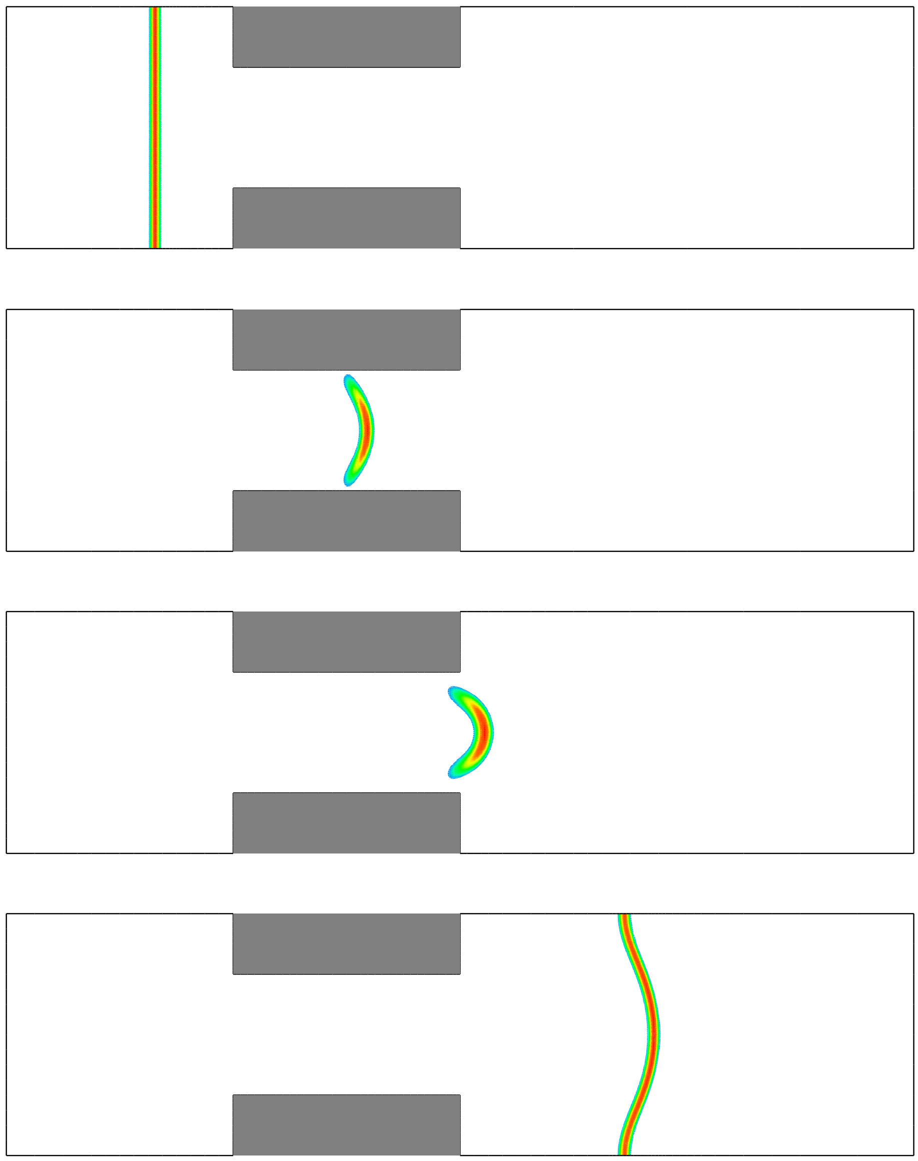

Fig. 2. Flame through cooled grid, $Le = 1$, $k = 0.1$. Reaction rate at $t = 1, 20, 40, 60$.

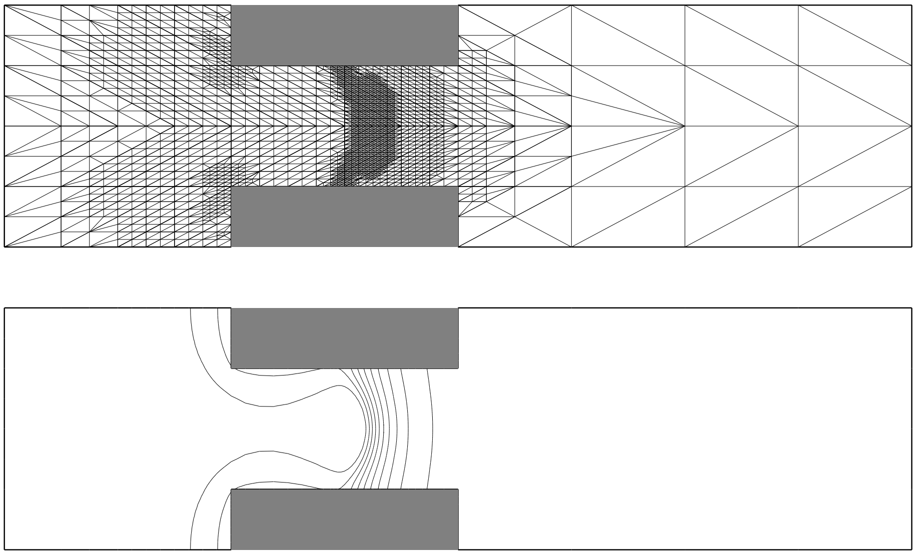

FIG. 3. Flame through cooled grid, $Le = 1$, $k = 0.1$. Grid and lines of constant temperature at $t = 20$ (corresponding to the second picture from above in Fig. 2).

would furthermore have to be adjusted by hand savely below the limit for stability and precision. The peaks in this diagram pointing to small values are related to the fact that a plot at a prescribed time t has been requested. This generally imposes one very small time step to exactly reach this point. Handling this is not straightforward with the estimation procedure for the timestep described in section 3. We therefore restarted with a given time step surely below the required one (a modified estimation scheme might be used as well). The figure thus permits to appreciate the rapidity and robustness of the temporal adaption which returns to the optimal value in about two steps.

In contrast to the computation with $k = 0.1$ the flame is extinguished in the obstacle for $k = 0.2$ (Fig. 5). The final state exhibits a broad region of non–vanishing reaction rate but with maximal value three orders of magnitude below the one at $t = 1$. It is controlled by the diffusion of species towards the reaction zone and highly depends on the boundary condition on the left hand side. Observe the phase of extinction between $t = 7$ and $t = 27$ being monitored by a linear decay of the overall reaction rate in Fig. 6. When approaching the final state the large distance between the symbols (representing one time step each) reveals that indeed a very large time step is being chosen in this phase.

4 Reaction front in a solid

The second class of problems that we will deal with refers to solid-solid combustion. The particularity of such a process is that convection is impossible and that the macroscopic

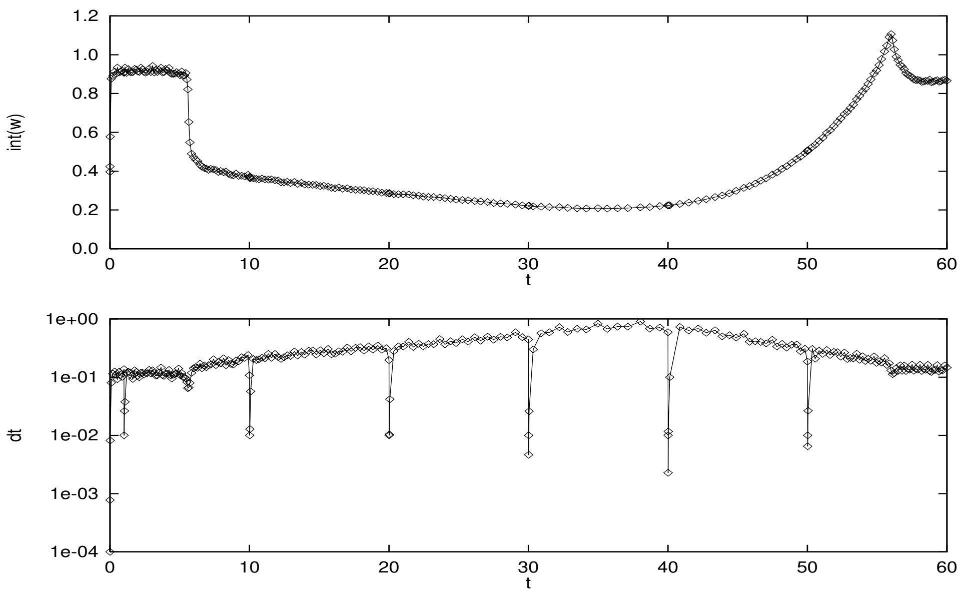

FIG. 4. Flame through cooled grid, $Le = 1$, $k = 0.1$. Evolution of total reaction rate and time step.

diffusion for the species in solids is in general negligible with respect to heat conductivity. With the heat diffusion time scale as reference the equations for a one step chemical alloying reaction read

$$\partial_t T \;-\; \kappa \nabla^2 T \;=\; Q\omega \qquad (4.1)$$

$$\partial_t Y \;=\; -\omega \qquad (4.2)$$

where T is the temperature divided by a reference temperature, Y the concentration of the deficient reactant and Q a heat release parameter. Concerning the reaction term quite a number of different modells are employed in the literature. They generally contain an Arrhenius term for the temperature dependence and use a first order reaction i.e.

$$\omega \;=\; K_0\, Y\, e^{-\frac{E}{T}} \qquad (4.3)$$

where E is a dimensionless activation energy. Since this expression is difficult to treat with analytical approaches it is often replaced by a zero–order mechanism substituting Y in (4.3) by $\chi(Y) = H(Y)$, the Heaviside function [MV94]. Although simpler, this expression involves an additional modelling and furthermore might generate difficulties in the numerical solution due to the discontinuity of χ.

Realistic processes involve apart from the reaction other physical mechanisms such as melting which leads to additional heat release (e.g. [BM87]) or microscopic diffusion of the reactant into the fine grains constituting the material. Smooke and Koszykowski [SK86] employ

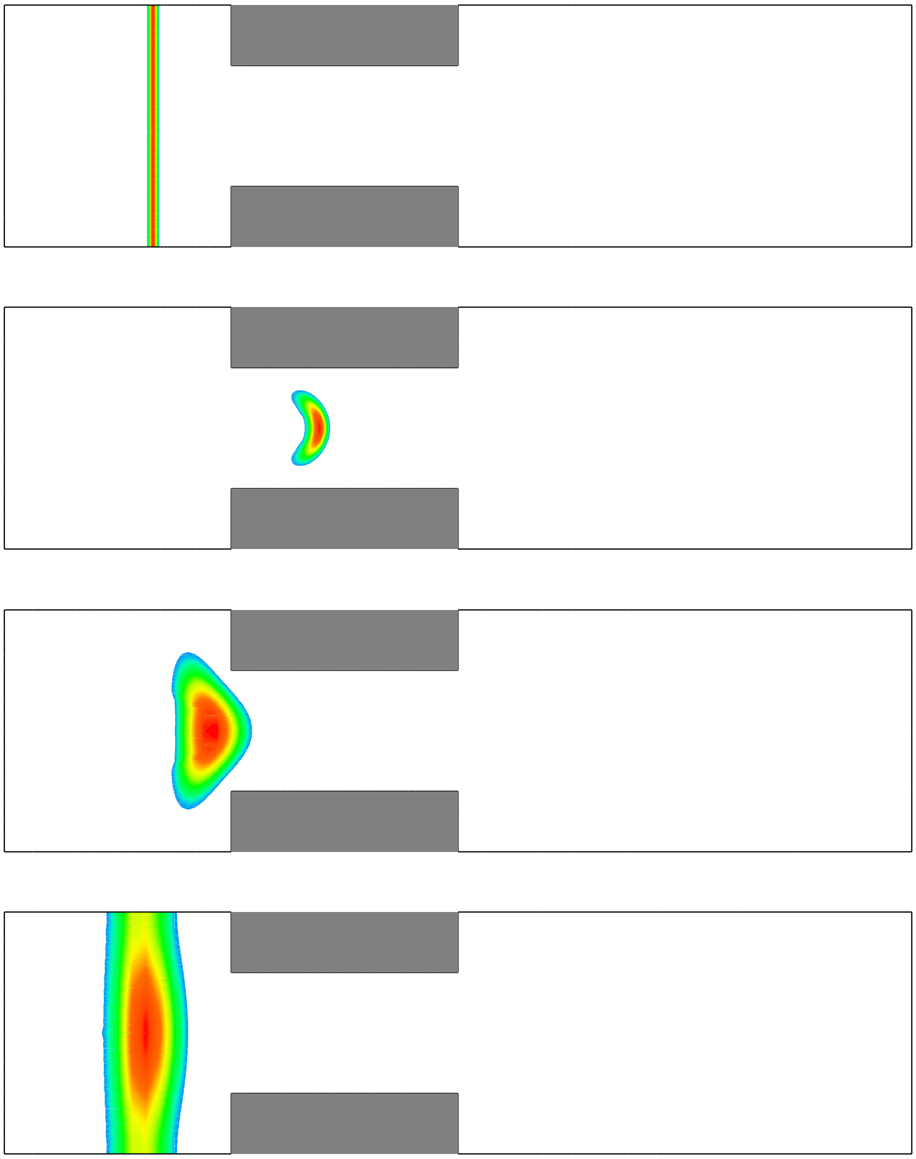

FIG. 5. Flame through cooled grid, $Le = 1$, $k = 0.2$. Reaction rate at $t = 1, 20, 40, 100$ (scale adapted to instantaneous range of values).

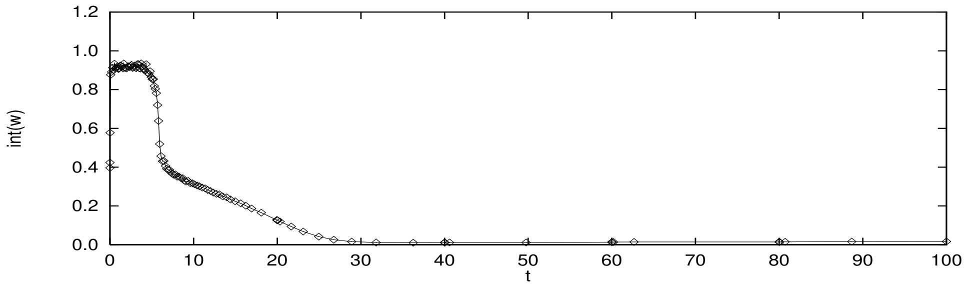

FIG. 6. Flame through cooled grid, $Le = 1$, $k = 0.2$. Evolution of total reaction rate.

$$\omega(T,Y) = \frac{D}{R^2}\,F(Y)\,e^{-\frac{E}{T}} \quad , \qquad F(Y) = \frac{Y^{1/3}}{1 - Y^{1/3}} \tag{4.4}$$

which has been developed by Booth [Boo53] considering a material made up of densly packed spheres subject to melting and microscopic diffusion of the reactant. Here, R is the radius of the spheres and D a microscopic diffusion coefficient. Due to the absence of macroscopic species diffusion and the related smoothing property the system (4.1), (4.2) is more difficult to treat numerically than the thermodiffusive equations. Nevertheless the same algorithm could be employed.

In our computations we experienced the need to adjust the term F in (4.4) to finite precision numerical treatment. This is justified, since, after all, (4.4) can just be a model of limited validity. First, the maximal range for Y is by definition the interval $[0,1]$. However, $F(1)$ can not be evaluated. For global conservation the physical range in fact is $[0, Y_I]$ where Y_I is the maximum value of the initial condition. Hence, choosing $Y(x,0) = 0.999$ instead of 1 [SK86] removes this difficulty. Second, the employed spatial approximation does not guarantee that Y remains within a certain interval. Therefore $F(Y)$ has been replaced by the tangent at $Y = 0.999$ and $Y = 0.001$ to the right and to the left of these values, respectively. This prolongation of $\omega(T,Y)$ to arguments Y outside the original range of definition $[0,1]$ results in a value of ω which brings the solution back to the physically meaningful range in case of overshooting due to finite precision. Such minor adjustments although much smaller than the accuracy of the model may decide on the failure or the success of a computation. In different practical computations both authors have experienced this strategy to be much more robust than e.g. replacing overshoots by the physically limiting values. This is particularly important when adaptive discretization is used which has less tendency to attenuate fine scale oscillations.

In the following we report on the solution of (4.1), (4.2), (4.4) for a non–uniformly packed solid in cylindrical geometry. We consider the value of D/R^2 being equal to 5800 within a circle of radius $r_1 = 0.0018$ and to increase linearly up to 16 times this

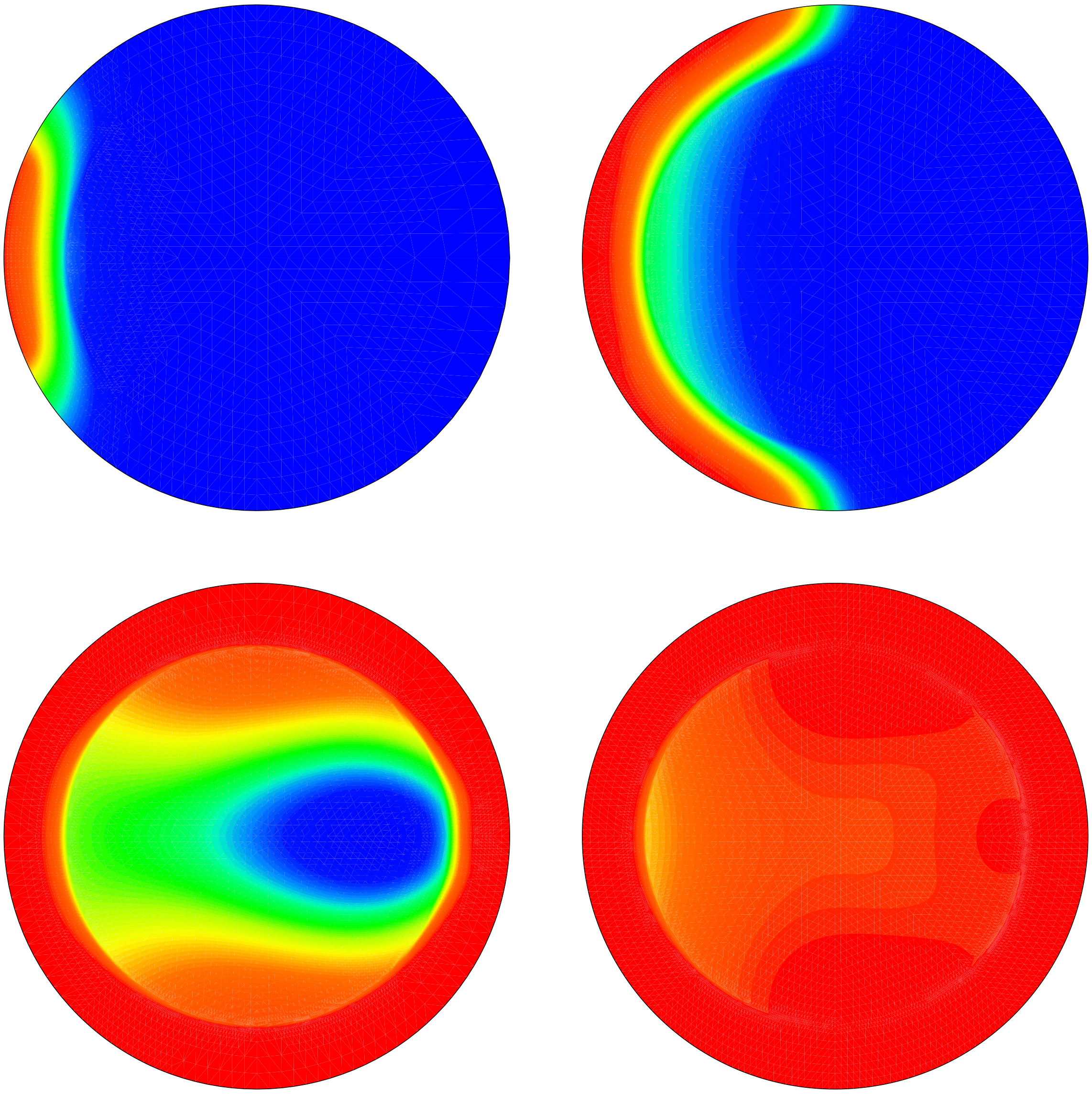

FIG. 7. Non–uniformly packed solid. Concentration of the reactant at times $t = 0.05$, 0.065, 0.07, 0.072. In these pictures dark black corresponds to the unburnt state, light color to intermediate states, and gray to completed reaction.

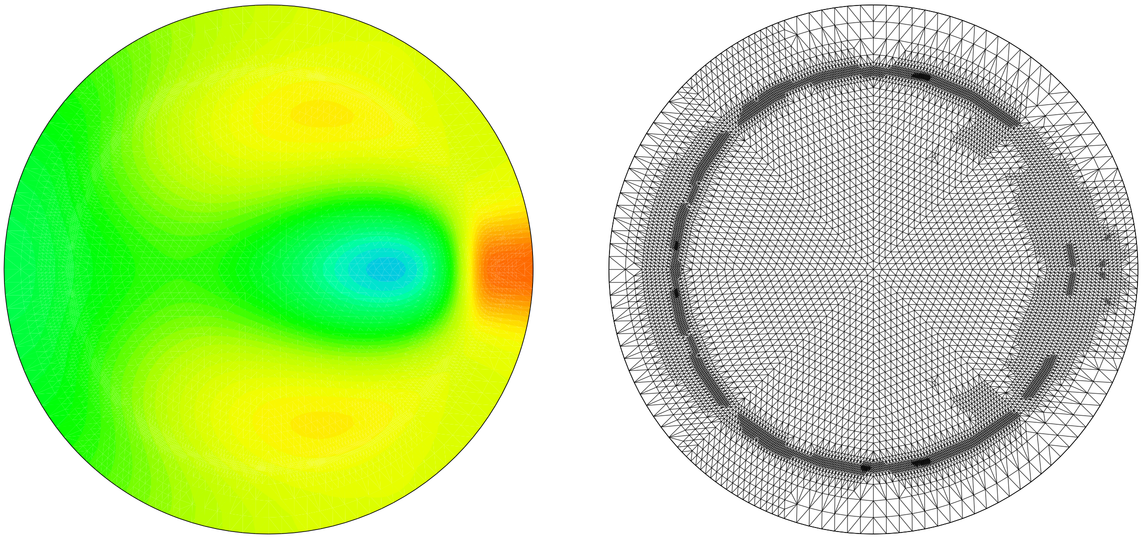

FIG. 8. Non–uniformly packed solid. Temperature and grid at $t = 0.07$.

value at $r_2 = 0.0024$. This yields a strongly increased flame velocity close to this radius which constitutes the outer border. The reactor is ignited by a Dirichlet condition $T_w = 300 + 24000\,t,\ t < 0.05$, for the wall temperature on a 45 degrees section of the boundary on the left hand side. For $t \geq 0.05$ and all other locations the boundary conditions are homogeneous Neuman conditions. Further parameters are $E = 11000$, $\kappa = 0.0001$, $Q = 2700$. Fig. 7 nicely illustrates how the reaction front first propagates along the outer wall before entering the core. The graphs should be related to those of Fig. 9 revealing that the reaction phase is rather short compared to the ignition. The small time steps at $t = 0.05$ result from the requirement of exactly attaining this instant where the boundary conditions are modified. Even in this simple geometry the interaction of different fronts can generate a rather complicated pattern in space and time. The reaction rate for example exhibits a peak where both peripherical fronts have merged and propagate into the interior whereas the maximum of the temperature appears at a later time.

Having mainly concentrated on the temporal adaptivity in the previous section we like to focus more on the spatial adaptivity for this second example. Fig. 8 shows temperature and grid at $t = 0.07$ to complement Fig. 7. Due to heat conduction the temperature is distributed much smoother than Y. Here it becomes obvious that an appropriate norm for the solution vector is an important ingredient in an adaptive refinement procedure for a system of PDEs. The norm defined by (2.8),(2.9) is able to account for very disparate length scales and scaling of the different components. In the present case it is mainly the steepness of Y requiring the observed refinement whereas temperature and reaction rate (not depicted here) have a completly different behaviour. Of course, being smoother, they are duely represented on this grid as well. From Fig. 9 it is finally obvious that

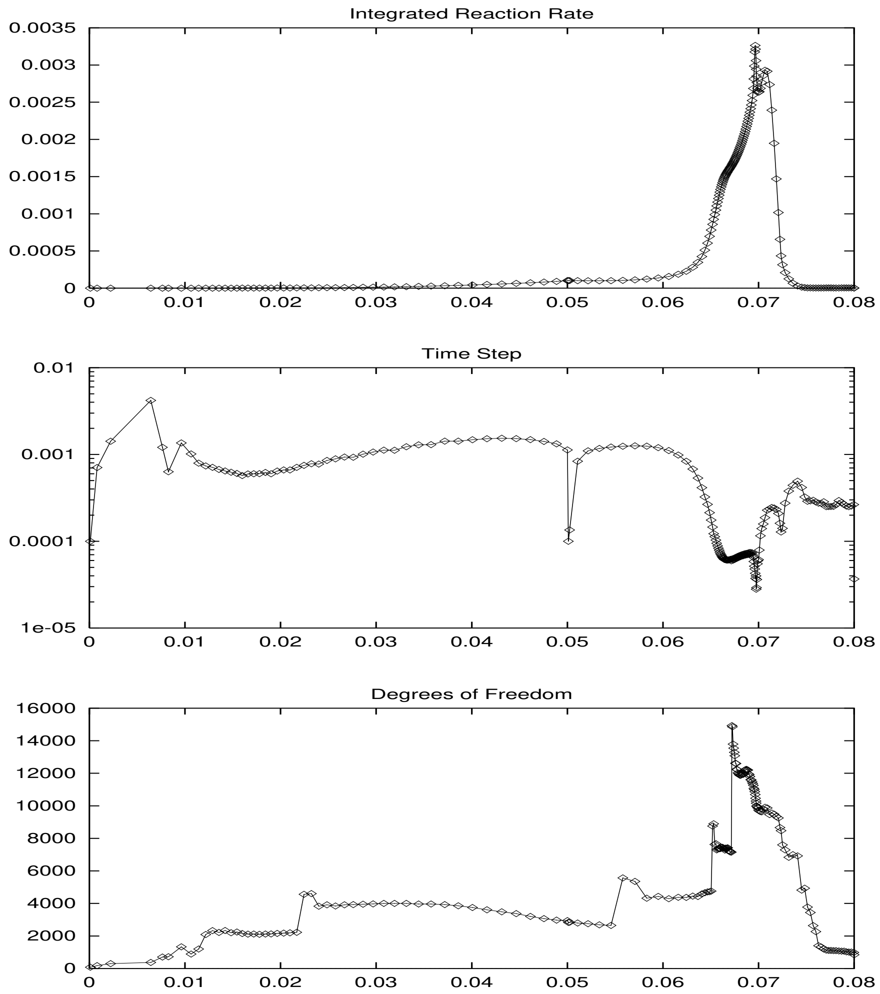

FIG. 9. Non–uniformly packed solid. Temporal evolution of the total reaction rate $\int \omega d\Omega$, the time step $\triangle t$, and the number of nodes N for $TOL = 1.5\,10^{-3}$.

practically relevant problems of the present type can adequately be resolved with the proposed method using not more than about 15000 nodes.

Acknowledgement

The authors wish to thank P. Deuflhard for inspiring discussions on stiff ODE integrators and adaptive multilevel methods. Furthermore, R. Roitzsch is acknowledged for his long term support during the implementation of the code and U. Maas for constructive remarks in the course of this work.

References

[AF88] S. Adjerid and J. E. Flaherty. Second–Order Finite Element Approximations and A Posteriori Error Estimation for Two–Dimensional Parabolic Systems. *Numer. Math.*, 53:183–198, 1988.

[BA76] I. Babuška and A. K. Aziz. On the angle condition in the finite element method. *SIAM J. Numer. Anal.*, 13:214–226, 1976.

[BB82] M. Bieterman and I. Babuška. The Finite Element Method for Parabolic Equations I: A posteriori Error Estimates. *Numer. Math.*, 40:339–371, 1982.

[BDL89] F. Benkaldoun, B. Denet, and B. Larrouturou. Numerical Investigation of the Extinction Limit of Curved Flames. *Combust. Sci. and Tech.*, 64:187–198, 1989.

[BF70] W.B. Bush and F.E. Fendel. Asymptotic Analysis of Laminar Flame Propagation for general Lewis Number. *Combust. Sci. and Tech.*, 1:421–428, 1970.

[BM87] A. Bayliss and B.J. Matkowsky. Fronts, Relaxation Oscillations, and Period Doubling in Solid Fuel Combustion. *J. Comp. Phys.*, 71:147–168, 1987.

[Boo53] F. Booth. The Theory of Self–Propagating Exothermic Reactions in Solid Systems. *Trans. Faraday Soc.*, 49:272–281, 1953.

[Bor92] F.A. Bornemann. An Adaptive Multilevel Approach to Parabolic Equations III. 2D Error Estimation and Multilevel Preconditioning. *IMPACT Comput. Sci. Engrg*, 4:1–45, 1992.

[BR78] I. Babuška and W.C. Rheinboldt. A Posteriori Error Estimates for the Finite Element Method. *Int. J. Numer. Meth. in Eng.*, 12:1597–1615, 1978.

[BS90] I. Babuška and M. Suri. The p and h–p versions of the Finite Element Method, An Overview. *Comp. Meth. Appl. Mech. Engrg.*, 80:5–26, 1990.

[BW85] R.E. Bank and A. Weiser. Some A Posteriori Estimators for Elliptic Partial Differential Equations. *Math. Comp.*, 44:283–301, 1985.

[DH92] B. Denet and P. Haldenwang. Numerical Study of Thermal-Diffusive Instability of Premixed Flames. *Combust. Sci. and Tech.*, 86:199–221, 1992.

[DLN96] P. Deuflhard, J. Lang, and U. Nowak. Adaptive Algorithm in Dynamical Process Simulation. In *Proceedings of the 8th ECMI Conference Sept. 1994 Kaiserslautern*. Teubner, 1996.

[DLP89] A. Dervieux, B. Larrouturou, and R. Peyret. On some Adaptive Numerical Approaches of Thin Flame Propagation Problems. *Computers & Fluids*, 17:39–60, 1989.

[DLY89] P. Deuflhard, P. Leinen, and H. Yserentant. Concepts of an Adaptive Hierarchical Finite Element Code. *IMPACT Comput. Sci. Engrg.* , 1:3–35, 1989.

[ELR93] B. Erdmann, J. Lang, and R. Roitzsch. KASKADE Manual - Version 2.0. Technical Report TR 93-5, Konrad-Zuse-Zentrum für Informationstechnik Berlin, 1993.

[FP91] J. Fröhlich and R. Peyret. A Spectral Algorithm for Low Mach Number Combustion. *Comp. Meth. Appl. Mech. Eng.*, 90:631–642, 1991.

[FS95] J. Fröhlich and K. Schneider. An adaptive Wavelet–Vaguelette Algorithm for the Solution of Nonlinear PDEs. Technical Report SC 95-28, Konrad-Zuse-Zentrum für Informationstechnik Berlin, 1995.

[Gus92] K. Gustafsson. *Control of error and convergence in ODE solvers.* PhD thesis, Department of Automatic Control, Lund Institut of Technology, Lund, Sweden, 1992.

[HW91] E. Hairer and G. Wanner. *Solving Ordinary Differential Equations II, Stiff and Differential–Algebraic Problems*, volume 14 of *Springer Series in Computational Mathematics.* Springer-Verlag, 1991.

[Lan95] J. Lang. Two-dimensional fully adaptive solutions of reaction–diffusion equations. *Appl. Numer. Math.*, 18:223–240, 1995.

[Lan96] J. Lang. High–resolution selfadaptive computations on chemical reaction–diffusion problems with internal boundaries. *Chem. Engrg. Sci.*, 51:1055–1070, 1996.

[LW92] J. Lang and A. Walter. A Finite Element Method Adaptive in Space and Time for Nonlinear Reaction-Diffusion Systems. *IMPACT Comput. Sci. Engrg.* , 4:269–314, 1992.

[Mit89] W.F. Mitchell. A comparison of Adaptive Refinement Techniques for Elliptic Problems. *ACM Trans. on Math. Software*, 15:326–347, 1989.

[Moo94] P. K. Moore. A Posteriori Error Estimation with Finite Element Semi– and Fully Discrete Methods for Nonlinear Parabolic Equations in One Space Dimension. *SIAM J. Numer. Anal.*, 31:149–169, 1994.

[MV94] B.J. Matkowsky and V. Volpert. Spiral Gasless Condensed Phase Combustion. *SIAM J. Appl. Math.*, 54:132–146, 1994.

[NB87] A. K. Noor and I. Babuška. Quality assessment and control of finite element solutions. *Finite Element Anal. Des.*, 3:1–26, 1987.

[Pet82] N. Peters. Discussion of Test Problem A. In N. Peters and J. Warnatz, editors, *Numerical Methods in Laminar Flame Propagation, Notes on numerical fluid mechanics, Vol. 6*, pages 1–14. Vieweg, 1982.

[PW82] N. Peters and J. Warnatz, editors. *Numerical Methods in Laminar Flame Propagation, Notes on numerical fluid mechanics, Vol. 6.* Vieweg, 1982.

[Roc88] M. Roche. Rosenbrock Methods for Differential Algebraic Equations. *Numer. Math.*, 52:45–63, 1988.

[SK86] M.D. Smooke and M.L. Koszykowski. Two-Dimensional Fully Adaptive Solutions of Solid-Solid Alloying Reactions. *J. Comp. Phys.*, 62:1–25, 1986.

[Ver94] R. Verfürth. A posteriori Error Estimation and Adaptive Mesh–Refinement Techniques. *J. Comp. Appl. Math.*, 50:67–83, 1994.